Mapping substrate/film adhesion with contact-resonance-frequency atomic force microscopy

D. C. Hurley,[a] M. Kopycinska-Müller, E. D. Langlois, A. B. Kos, and N. Barbosa III
National Institute of Standards and Technology, Boulder, Colorado 80305

(Received 28 March 2006; accepted 23 May 2006; published online 12 July 2006)

We have used contact-resonance-frequency atomic force microscopy techniques to nondestructively image variations in adhesion at a buried interface. Images were acquired on a sample containing a 20 nm gold (Au) blanket film on silicon (Si) with a 1 nm patterned interlayer of titanium (Ti). This design produced regions of very weak adhesion (Si/Au) and regions of strong adhesion (Si/Ti/Au). Values of the contact stiffness were 5% lower in the regions of weak adhesion. The observed behavior is consistent with theoretical predictions for layered systems with disbonds. Our results represent progress towards quantitative measurement of adhesion parameters on the nanoscale. [DOI: 10.1063/1.2221404]

Control of the adhesion between a thin film and its substrate is crucial to the yield, performance, and reliability of devices in a myriad of applications (e.g., microelectronics[1]). Although this statement has been true for several decades,[2] the situation today may be judged more pressing for two reasons. First, the current drive towards smaller length scales means that established methods to determine adhesion often possess inadequate spatial resolution. Second, it is increasingly important to image or visualize the spatial distribution in mechanical properties such as adhesion, rather than obtaining "average" or "typical" values from a single position.

Existing methods to determine mechanical properties with micro- to nanoscale spatial resolution include nanoindentation[3,4] and scanning acoustic microscopy.[5] However, the high spatial resolution and imaging capabilities of atomic force microscopy (AFM) make it a promising method for nanoscale materials characterization. One subset of AFM methods that provides mechanical-property information is an emerging group of contact techniques in which the cantilever is vibrated at or near the frequencies of its resonant modes. Techniques such as atomic force acoustic microscopy (AFAM),[6,7] ultrasonic AFM,[8] and ultrasonic force microscopy[9,10] have been used to evaluate mechanical properties and associated effects including elastic modulus,[6–9] subsurface defects,[10–12] and friction.[13] Here, we demonstrate how such methods can be used to detect and image variations in thin-film adhesion at a buried interface. Unlike methods that merely yield qualitative or relative property indications, contact-resonance-frequency imaging provides quantitative information about near-surface properties. These images are the first step toward the ultimate goal of quantitative imaging—mapping—of adhesion parameters on the nanoscale.

Our methods are based on the AFAM technique,[14,15] which involves vibrating the sample at frequencies in the range from 100 kHz to 3 MHz by means of a piezoelectric transducer beneath the sample. When the tip of the AFM cantilever is in contact with the sample and the transducer vibrations have the appropriate frequency, resonant modes of the cantilever are excited. The values of these "contact-resonance frequencies" are determined by monitoring the amplitude of cantilever vibration as a function of excitation frequency. From the contact-resonance frequencies, the tip-sample contact stiffness k^* is calculated with the help of suitable models for the cantilever beam dynamics. Sample properties such as elastic modulus are obtained from k^* by use of models for the tip-sample contact mechanics. It is important to note that AFAM experiments probe the sample properties to a depth z roughly three times that of the tip-sample contact radius a. For Hertzian contact mechanics, $a=(3RF/4E^*)^{1/3}$, where R is the tip radius of curvature, F is the applied static force, and $E^*=(1/M_t+1/M_s)^{-1}$ is the system reduced modulus determined by the indentation moduli M_t of the tip and M_s of the sample.[16] For $z>3a$, the stress field beneath the tip[16] is sufficiently small relative to the value at the surface ($<10\%$) that the measurement is not sensitive to property variations. In this way, the relative depth sensitivity of AFAM is affected by the choice of experimental parameters R and F.

For quantitative imaging with AFAM principles, we have developed frequency-tracking electronics to detect and record the contact-resonance frequency at each image location. Other approaches have also been demonstrated.[6,17–19] Our techniques were previously described in the context of quantitative modulus mapping[7] and are based on a digital signal processor architecture. The circuit applies a swept-frequency sinusoidal voltage to the piezoelectric transducer under the sample. A rms-to-dc converter (bandwidth from 1 kHz to 3.2 MHz) detects the amplitude of the AFM photodiode signal and supplies it to an analog-to-digital converter. From the rms voltage versus frequency response, the circuit determines the frequency of maximum amplitude (peak frequency). This frequency determines the voltage sent to the AFM auxiliary input port for image acquisition. The acquired voltage image thus represents the value of the contact-resonance frequency at each position. Digitizing at 48 kilosamples per second and recording 128 samples per spectrum, the current system can acquire a complete spectrum every 2.7 ms. The AFM scan speed must be adjusted to ensure that several spectrum sweeps are made at each image position. For scan lengths up to several micrometers, an image with 256×256 pixels can usually be acquired in 20–25 min.

[a]Electronic mail: hurley@boulder.nist.gov

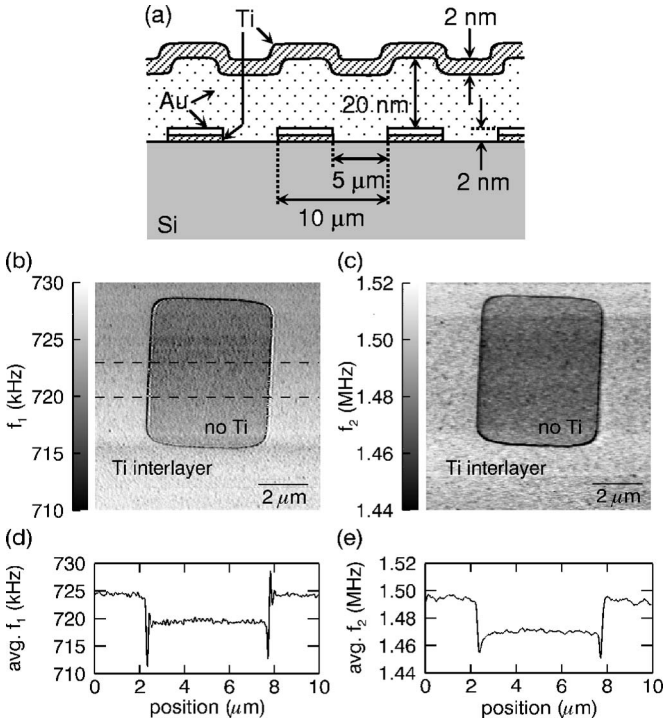

FIG. 1. (a) Schematic of model film-adhesion sample in cross section. [(b) and (c)] Contact-resonance-frequency images of the cantilever's first and second flexural modes f_1 and f_2, respectively. [(d) and (e)] Average frequency vs position across the center of the images in (b) and (c), respectively. The dashed lines in (a) indicate the image region used to obtain the averages.

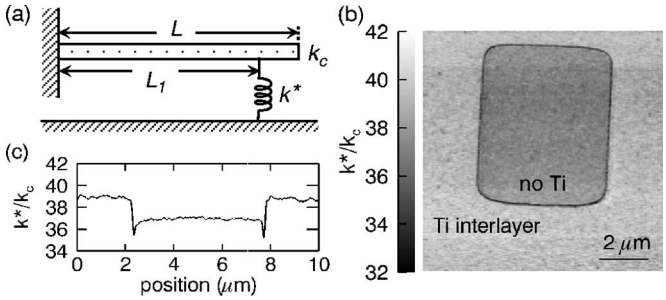

FIG. 2. (a) Model for cantilever dynamics. (b) Image of the normalized contact stiffness k^*/k_c calculated from the contact-resonance-frequency images in Fig. 1. (c) Average stiffness vs position across the center of the image in (b).

To experimentally investigate substrate/film adhesion, we fabricated a model system of gold (Au) and titanium (Ti) thin films on (001) single-crystal silicon (Si). These materials were chosen because noble metals such as Au typically have very poor adhesion to substrates such as Si, but interlayers of oxygen-active metals such as Ti greatly improve that adhesion.[2] Figure 1(a) shows a cross-sectional schematic of the sample design. A rectangular array of 5×5 μm^2 squares (10 μm pitch) of Au/Ti surrounded by a grid of Ti/Au/Ti was created on the Si wafer in the following manner. Prior to film deposition, the polished wafer was first etched to remove its native oxide. A lift-off resist pattern was applied using standard photolithography to form the array. The wafer was subjected to an oxygen plasma ash to remove any residual resist in the areas not fully cleared by the development process. A 1 nm Ti/1 nm Au bilayer was then electron-beam evaporated without breaking vacuum. The Au layer ensured a good bond between the Ti and the overlying Au layer by preventing any oxidation of the Ti surface when exposed to ambient pressure. After deposition, the lift-off resist was chemically stripped and a second oxygen plasma ash was applied. A 20 nm blanket film of Au was then electron-beam evaporated. Finally, a 2 nm Ti topcoat layer was deposited without breaking vacuum. This Ti layer provided a hard surface for the AFM tip and prevented contamination of the tip by the soft Au film.

This process was intended to produce a sample with minimal variations in topography and composition at the surface, but with variations in the adhesion of a buried interface. We performed a crude scratch test by lightly dragging one end of a tweezers across the film surface. Under an optical microscope, it was clear that this treatment had removed the film in the scratched regions without a Ti interlayer (squares) and remained intact in the scratched regions containing a Ti interlayer (grid). This result confirms our assumptions about the relative adhesion of the different sample regions.

Figures 1(b) and 1(c) show contact-resonance-frequency images for the first (f_1) and second (f_2) flexural modes, respectively. The images were acquired using a rectangular, single-crystal Si cantilever with length $L=230\pm5$ μm, width $b=40\pm3$ μm, and thickness $t=7.0\pm0.5$ μm. The measured free-space resonant frequencies for the lowest two flexural modes were $f_1=165.09\pm0.01$ kHz and $f_2=1061.61\pm0.01$ kHz. The value $Q=971\pm20$ was measured for the quality factor of f_1. Using the above values for L, b, f_1, and Q, we calculate a value for the cantilever spring constant $k_c=46\pm4$ N/m using the method of Sader *et al.*[20] The images were acquired at a cantilever deflection of $\delta=20\pm1$ nm. Therefore, the static force applied during imaging was $F=k_c\delta=0.92\pm0.09$ μN.

The roughly square feature in each image corresponds to a region of weak adhesion. (Drift in the AFM scanners may be the reason why this feature does not appear to be perfectly square in the image.) The thin lines surrounding the square indicate relatively large, topography-induced frequency shifts. The shifts are most likely caused by transient changes in the contact area at the edges of the square. Therefore, the frequency data in these regions are not considered reliable. Otherwise, the values of f_1 and f_2 are very uniform and repeatable from line to line. The images show that the contact-resonance frequency is noticeably lower for the region of weak adhesion. Figures 1(d) and 1(e) contain the average frequency versus scan position for Figs. 1(b) and 1(c), respectively. Each line scan was created by averaging 40 lines in the center of the corresponding image. The scans show that the average frequency of f_1 is about 5 kHz lower inside the square (719.7 ± 2.4 kHz vs 724.8 ± 2.5 kHz), while for f_2 the average frequency drops by 25 kHz (1.472 ± 0.006 MHz vs 1.497 ± 0.008 MHz). The average shift in frequency for each mode depends not only on the relative difference in material properties, but also on the sensitivity of each mode,[21] which is determined by the specific combination of experimental parameters (R, F, etc.).

To further analyze our results, we used the frequency images in Figs. 1(b) and 1(c) to obtain a contact-stiffness image. The image was calculated with an analytical model for the cantilever beam dynamics.[14,15] As shown in Fig. 2(a), this model contains a cantilever represented by a rectangular beam of length L that is clamped at one end. The cantilever has a spring constant k_c and its mass is distributed along its

length. The tip is located a distance L_1 from the clamped end of the cantilever. For purely elastic forces, the tip-sample interaction is represented by a spring of stiffness k^*.

The image of the normalized contact stiffness k^*/k_c calculated from the contact-resonance-frequency images is shown in Fig. 2(b). Consistent with the frequency images, the contact stiffness is lower inside the square. A line scan of the average value of k^*/k_c versus position obtained from the same 40 lines as used for Figs. 1(d) and 1(c) is shown in Fig. 2(c). The mean value of k^*/k_c is 39.1 ± 0.6 in the grid regions and 37.1 ± 0.5 in the square, a difference of 5%. We analyzed several other pairs of contact-resonance-frequency images acquired at different sample positions. The resulting contact-stiffness images consistently showed a decrease of 4%–5% in k^*/k_c for the regions of poor adhesion that lacked a Ti interlayer.

Our results provide direct experimental support for previously published predictions of reduced contact stiffness in layered systems containing disbonds.[22] An impedance-radiation theory was used in which the disbonded substrate/film interface was modeled by a change in boundary conditions (i.e., zero shear stress at the interface). With this approach, Ref. 22 predicted that for a disbond in a 20–25 nm aluminum film ($M=78$ GPa) on (100) Si ($M=165$ GPa), the contact stiffness would be lower by ~4%, very similar to our observed reduction of 5%. The two results cannot be directly compared for several reasons, however. The film materials are different, although not dramatically dissimilar elastically. [For our sample, $M(\mathrm{Au})=97$ GPa and $M(\mathrm{Ti})=129$ GPa.[23]] Our sample also contained additional (albeit very thin) film layers. Finally, in our experiments the estimated static load $F=0.92$ μN and tip radius $R \approx 20-50$ nm, while the calculations assumed $F=0.2$ μN and $R=100$ nm. However, it is the product FR that affects the contact radius a and thus k^*. Using the equation for a given above, we find $a=6-8.5$ nm for our experimental parameters. These estimates include the effect of the thin Ti layers through the use of an effective (weighted) modulus for the film. For the parameters used in Ref. 22, we obtained $a=6.6$ nm. The similarity in the values for a leads us to believe that comparison between the model and our experiments is valid, and that weak adhesion is responsible for our experimental results.

In summary, we have demonstrated how contact-resonance-frequency AFM imaging can be used to nondestructively map variations in adhesion at a substrate/film interface. A model system containing regions of both weak and strong adhesions was fabricated with Au and Ti films on Si. Images of the two lowest flexural-mode, contact-resonance frequencies were acquired and used to calculate a map of the tip-sample contact stiffness. Values of the contact stiffness were 5% lower in the regions of weak adhesion. The observed behavior is consistent with theoretical models for contact stiffness in layered systems with disbonds. Our results represent progress towards the goal of nanoscale mapping of adhesion, which will significantly impact development of thin-film devices in a wide range of technological applications.

The authors thank G. C. Hilton (NIST) and R. R. Keller (NIST) for valuable discussions.

[1] *International Technology Roadmap for Semiconductors*, http://public.itrs.net
[2] B. N. Chapman, J. Vac. Sci. Technol. **11**, 106 (1974).
[3] W. C. Oliver and G. M. Pharr, J. Mater. Res. **7**, 1564 (1992).
[4] S. A. Syed Asif, K. J. Wahl, R. J. Colton, and O. L. Warren, J. Appl. Phys. **90**, 1192 (2001).
[5] J. D. Achenbach, J. O. Kim, and Y.-C. Lee, in *Advances in Acoustic Microscopy*, edited by G. A. D. Briggs (Plenum, New York, 1995), Vol. 1, Chap. 5, pp. 153–208; Z. Sklar, P. Mutti, N. C. Stoodley, and G. A. D. Briggs, *ibid.*, Vol. 1, Chap. 6, pp. 209–248.
[6] U. Rabe, M. Kopycinska, S. Hirsekorn, J. Muñoz Saldaña, G. A. Schneider, and W. Arnold, J. Phys. D **35**, 2621 (2002).
[7] D. C. Hurley, M. Kopycinska-Müller, A. B. Kos, and R. H. Geiss, Meas. Sci. Technol. **16**, 2167 (2005).
[8] T. Tsuji, S. Saito, K. Fukuda, K. Yamanaka, H. Ogiso, J. Akedo, and K. Kawakami, Appl. Phys. Lett. **87**, 071909 (2005).
[9] R. E. Geer, O. V. Kolosov, G. A. D. Briggs, and G. S. Shekhawat, J. Appl. Phys. **91**, 4549 (2002).
[10] A. P. McGuigan, B. D. Huey, G. A. D. Briggs, O. V. Kolosov, Y. Tsukahara, and M. Yanaka, Appl. Phys. Lett. **80**, 1180 (2002).
[11] T. Tsuji and K. Yamanaka, Nanotechnology **12**, 301 (2001).
[12] G. S. Shekhawat and V. P. Dravid, Science **310**, 89 (2005).
[13] M. Reinstädtler, U. Rabe, V. Scherer, J. A. Turner, and W. Arnold, Appl. Phys. Lett. **82**, 2604 (2003).
[14] U. Rabe, S. Amelio, E. Kester, V. Scherer, S. Hirsekorn, and W. Arnold, Ultrasonics **38**, 430 (2000).
[15] D. C. Hurley, K. Shen, N. M. Jennett, and J. A. Turner, J. Appl. Phys. **94**, 2347 (2003).
[16] K. L. Johnson, *Contact Mechanics* (Cambridge University Press, Cambridge, 1985), pp. 93–94.
[17] K. Yamanaka, Y. Maruyama, T. Tsuji, and K. Nakamoto, Appl. Phys. Lett. **78**, 1939 (2001).
[18] K. Kobayashi, H. Yamada, and K. Matsushige, Surf. Interface Anal. **33**, 89 (2002).
[19] E. Efimov and S. A. Saunin, http://www.ntmdt.ru/Publications/2002/
[20] J. Sader, J. W. M. Chon, and P. Mulvaney, Rev. Sci. Instrum. **70**, 3967 (1999).
[21] J. A. Turner and J. S. Wiehn, Nanotechnology **12**, 322 (2001).
[22] A. F. Sarioglu, A. Atalar, and F. L. Degertekin, Appl. Phys. Lett. **84**, 5368 (2004).
[23] G. Simmons and H. Wang, *Single Crystal Elastic Constants and Calculated Aggregated Properties: A Handbook* (MIT, Cambridge, 1971).